Journal of Photochemistry & Photobiology, B: Biology 281 (2026) 113494

Contents lists available at ScienceDirect

Journal of Photochemistry & Photobiology, B: Biology

journal homepage: www.elsevier.com/locate/jphotobiol

Enhanced blue-light antibacterial action of a neutral vanillin-derived polyimine against *Staphylococcus aureus*

Marilena Marino [a], Elisabetta Gover [b], Asja Brovedani [a], Robert C. Pullar [c], Daniele Goi [b], Francesco Andreatta [b], Alfredo Rondinella [b], Paolo Strazzolini [a], Clara Comuzzi [a,*]

[a] Department of Agricultural Food Environment and Animal Sciences, University of Udine, Via delle Scienze 206, 33100 Udine, Italy
[b] Polytechnic Department of Engineering and Architecture, University of Udine, Via del Scienze 206, Udine 33100, Italy
[c] Department of Molecular Sciences and Nanosystems, University Ca' Foscari Venice, Via Torino 155, 30172 Venezia Mestre, Venezia, (VE), Italy

ARTICLE INFO

Keywords:
Polyimine
Polymer–cell interactions
Antibacterial
Reusable polymer films

ABSTRACT

Microbial contamination remains a critical concern in water and biomedical contexts, motivating the search for sustainable disinfection strategies that minimize chemical inputs and energy demand. Blue light (400–470 nm) can inactivate bacteria via endogenous porphyrin photoactivation and reactive oxygen species (ROS) generation; however, significant antimicrobial effects typically require high fluences (>100 J cm^{-2}), **particularly at longer wavelengths such as 470 nm,** limiting practical applications. Therefore, strategies that lower the required dose without introducing exogenous photosensitizers are highly desirable. Here, we investigate the **previously reported** vanillin-derived polyimine (VP) as a **photo-inert interfacial modulator** of bacterial susceptibility to blue light. Although VP is not itself a photosensitizer, it enhances blue-light antibacterial efficacy against *Staphylococcus aureus* by inducing sublethal stress that increases susceptibility to endogenous photo-oxidative pathways. VP films alone did not reduce bacterial viability after 90 min of dark incubation, but colony morphology, growth kinetics, and scanning electron microscopy revealed the induction of sublethal cellular stress. When combined with 470 nm irradiation at moderate fluences (18–54 J cm^{-2}), selected to provide a weak light-only antibacterial action to reveal possible VP-mediated priming effects, VP films exhibited a reuse-dependent enhancement of antibacterial activity, with limited effect at first use and progressively stronger killing upon repeated reuse, ultimately approaching a 2-log reduction. Structural analyses (BET/BJH) showed that reuse-induced micro fracturing increased the specific surface area (12.9 m^2 g^{-1} for pristine films vs. 21.8 m^2 g^{-1} after reuse) without altering pore size distribution, thereby enhancing polymer–cell interactions. Importantly, no measurable generation of singlet oxygen, radical species, or hydrogen peroxide by the polymer was detected under the tested conditions, indicating that antibacterial activity arises from polymer-mediated sensitization of bacterial endogenous photo-oxidative pathways. Overall, these results support a *priming-plus-light* mechanism, in which a neutral polyimine induces sublethal physiological stress that amplifies bacterial susceptibility to blue-light irradiation under deliberately mild irradiation conditions.

1. Introduction

Microbial contamination represents a persistent challenge in water treatment, food, and biomedical settings, underscoring the need for innovative disinfection strategies that are efficient, non-toxic, and environmentally sustainable. Conventional methods, such as chlorination, thermal processing, or chemical biocides, can be highly effective but often have drawbacks, including chemical residues, energy demand, and the risk of promoting resistant strains [1]. Therefore, there is a growing interest in physical, non-thermal approaches capable of achieving reliable microbial control that meets sustainability criteria [2].

Light-based antimicrobial strategies are attracting increasing attention. UV-C radiation (200–280 nm) is well known for its germicidal action via direct nucleic acid damage and is currently applied in water, air, and surface disinfection [3,4]. However, its poor penetration, potential to generate toxicity, and safety management risks limit broader use [5,6]. These limitations are particularly relevant in aqueous systems,

* Corresponding author.
E-mail address: clara.comuzzi@uniud.it (C. Comuzzi).

https://doi.org/10.1016/j.jphotobiol.2026.113494
Received 6 February 2026; Received in revised form 15 May 2026; Accepted 3 June 2026
Available online 4 June 2026

where light penetration is a critical practical parameter. These drawbacks have shifted interest toward visible light. In particular, blue light (400–470 nm) can inactivate bacteria by exciting endogenous chromophores, primarily porphyrins and flavins, thereby generating intracellular ROS that damages membranes, proteins, and DNA [7,8]. In *S. aureus*, these endogenous photosensitizers are mainly intracellular porphyrins, primarily coproporphyrin III and protoporphyrin IX, which accumulate as intermediates of the heme biosynthetic pathway and act as efficient blue-light absorbers [9]. Upon excitation at 405–470 nm, they generate singlet oxygen and other ROS, providing a well-described intrinsic mechanism for blue-light susceptibility [10,11].

Unlike UV-C, blue light is generally considered safe for human exposure and compatible with many material surfaces. Its antimicrobial efficacy, however, is strongly dependent on irradiation parameters: wavelengths near 420–450 nm and fluences above 100 J cm^{-2} are typically required to achieve log-scale reductions in bacterial viability, whereas at longer wavelengths (e.g., 470 nm), the effect becomes markedly weaker [12–14]. Recent results show that this wavelength is effective against *S. aureus when applied at about 108–400 J* cm^{-2} [15]. To overcome this limitation, exogenous photosensitizers or chromophoric materials are often used to boost ROS formation under visible light [16–18]. Although effective, such strategies introduce additional constraints related to cost, photostability, and potential toxicological concerns. These limitations stimulate the search for synergistic approaches that enhance antimicrobial efficacy of blue light without relying on external photosensitizers, ideally through materials that modulate bacterial physiology to enhance endogenous photo-oxidative pathways.

Evidence from surface-based systems suggests that material properties can modulate bacterial susceptibility to light-induced oxidative stress. For instance, silver-nanoparticle coatings exhibit markedly enhanced antibacterial efficacy when combined with blue light [19], and visible-light-responsive TiO_2/g-C_3N_4 nanotube layers achieve improved microbial inactivation under irradiation conditions that are otherwise only weakly bactericidal [20]. Together, these studies, along with more recent work on photoactive antibacterial coatings and light-responsive surfaces, demonstrate that interfacial or structural features of a material can amplify light-driven antimicrobial effects, even when the matrix itself is not the primary source of ROS [19,20].

Polyimine-based materials have recently emerged as an intriguing class of antimicrobial polymers. Several studies have shown that polyimines derived from aromatic aldehydes or phenolic building blocks can inhibit the growth of both Gram-positive and Gram-negative bacteria. Their activity, however, is typically moderate and strongly contact-dependent, as imine-containing networks are reported to induce sublethal physiological stress rather than rapid bactericidal effects [21,22]. At the same time, previous studies have shown that bacterial cells subjected to sublethal stress conditions may become more susceptible to antimicrobial blue/violet light inactivation [23]. On this basis, we hypothesized that contact-dependent sublethal stress induced by polyimines could similarly sensitize bacterial cells to blue-light irradiation, thereby enhancing the antimicrobial outcome of visible-light treatment through altered cellular stress responses. ValPol (VP), a vanillin-derived polyimine recently developed in our laboratory [24], provides a suitable model system to explore this hypothesis. Originally introduced as an inert scaffold for immobilizing photosensitizers, VP is now used to test an alternative rationale: whether a neutral, photo-inert polyimine can nevertheless *prime* bacterial cells through contact-dependent sublethal stress, thereby increasing susceptibility to 470 nm irradiation. **Importantly, the novelty of the present work does not lie in the synthesis of a new polymer, but in the demonstration that this previously reported material can act as a contact-dependent physiological sensitizer under blue light.** In addition, because VP is processed as a reusable dynamic network, its surface accessibility may evolve during repeated cycles (e.g., through microfracturing), potentially strengthening polymer-cell interactions and amplifying the priming effect. Accordingly, the objectives of this work were to (i) quantify VP-induced sublethal stress in the dark, (ii) determine whether this priming enables a measurable enhancement of antibacterial activity at moderate 470 nm fluences (18–54 J cm^{-2}), selected to remain weakly effective in the absence of VP, thereby allowing the contribution of polymer-mediated priming to be resolved, and (iii) link reuse-dependent performance changes to the structural evolution of the films.

2. Materials and methods

2.1. Chemicals and culture media

All the chemicals employed were commercially available (Sigma-Aldrich Italia S.r.l., Milano, Italy) and used as received unless otherwise specified. Anhydrous K_2CO_3 was prepared by finely grinding the commercial powder and treating it at 250 °C for 8 h. Anhydrous ethane-1,2-diamine was obtained by distillation of the commercial reagent under inert atmosphere (Ar), collecting, and keeping over activated (300 °C, 8 h) 4 Å molecular sieves. Anhydrous *N,N*-dimethylformamide (DMF) was obtained from the commercial solvent, previously treated overnight with CaH_2 (5% m/v), at room temperature under stirring and inert atmosphere (Ar); decanted DMF was finally distilled (55 °C, 20 mmHg), collected, and kept over activated 4 Å molecular sieves (2 g in 10 mL). Brain Heart Infusion (BHI), Plate Count Agar (PCA) and Maximum Recovery Diluent (MRD) were purchased from Oxoid (Milan, Italy).

2.2. Microbial strain and culture conditions

Staphylococcus aureus strain 226 [25] was stored at −80 °C in BHI containing 30% glycerol. Before each trial, the strain was grown overnight in 1 mL of BHI at 37 °C. The cells were then recovered by centrifugation (5000 ×*g*, 4 °C), the pellet washed twice with Phosphate Buffered Saline (PBS) pH 7.4 and finally resuspended in 1 mL of PBS at a concentration of about 10^6 CFU mL^{-1}.

2.3. Syntheses

VP (Fig. S1) was synthesized according to the previously published procedure reported [24]. **Since the synthetic route and full physicochemical characterization of the material have already been described elsewhere, only the information necessary for reproducibility is briefly summarized here; the focus of the present study is on the biological and photobiological evaluation of VP [23].** Vanillin (12.6 g, 83.0 mmol) was dissolved in anhydrous DMF (50 mL) under stirring, and finely powdered anhydrous K_2CO_3 (26.26 g, 190.0 mmol) was added. 1,2-dibromoethane (8.22 mL, 17.85 g, 95.0 mmol) was introduced dropwise and the reaction mixture was maintained at 60 °C under argon for 4 h. After cooling, the suspension was poured into water (500 mL) and left at 4C overnight. The resulting solid was filtered, thoroughly washed with water, collected,and dried at 60 °C under reduced pressure over P_2O_5. The crude product was recrystallized from CH_3CN (450 mL) to afford the bis-aldehyde intermediate as colorless crystals.

The obtained bis-aldehyde (4.95 g, 15.0 mmol) was then dissolved in CH_2Cl_2 (375 mL) and treated with freshly distilled ethane-1,2-diamine (1.0 mL, 0.899 g, 15.0 mmol) at room temperature under magnetic stirring for 48 h in a sealed vessel. The white precipitate formed was filtered, washed, collected, and dried at 60 °C under reduced pressure in the presence of P_2O_5, yielding VP. Analytical and spectroscopic data (IR, NMR, MS) were consistent with previously reported ones [24]. The resulting powder, after a pretreatment with DMSO, was heated at 210 °C for 5 min to produce the final films. The obtained VP films were repeatedly immersed in sterile water before PDI trials in order to remove residual DMSO.

2.4. Microbial photoinactivation (PDI) trials

Irradiation experiments were performed using an array of LED-assembled lamps (TLWB7600, Telefunken Vishay, Torino, Italy), delivering blue light with an emission maximum at 470 nm [26,27]. Light intensity was carefully controlled by a power supply (Agilent Technologies Italy, Milano, Italy), and the fluence rate, set at 100 W m^{-2} for all the photooxidation experiments, was measured using an HD 2302.0 Light meter across the whole lamp area to ensure that each well was irradiated evenly (Delta OHM Srl, Padova, Italy).

PDI trials were carried out in wells of a 48-well flat-bottomed microplate (Corning Optical Communications Srl, Torino, I). 1 mL of *S. aureus* suspension in PBS was introduced into each well, then a 10 mm-diameter VP film was placed at the bottom of each well and remained fully immersed throughout the experiment. The plate was exposed to blue light for up to 90 min under magnetic stirring using a 6 × 3 mm cylindrical stirrer at 900 rpm. Control wells were also prepared containing 1 mL of cell suspension. One identical microplate was set up and kept in the dark for 90 min, and stirred in the same way as treated samples. The geometry of the LED source relative to the microplate was kept constant for all experiments to ensure uniform irradiation across the wells (Fig. S2).

During each PDI experiment, viable counts were determined at 30 min intervals using the drop-plate method [28]. Before sampling, the suspension was gently mixed to ensure homogeneous cell distribution. Serial decimal dilutions were prepared in MRD, and five 10 μL aliquots from each dilution were spotted in replicate onto PCA plates. Plates were incubated at 37 °C for 24 h, and counts were expressed as CFU mL^{-1}. After each PDI run, films intended for reuse were first thoroughly rinsed with water to remove residual medium and loosely associated biomass, then sanitized with ethanol and immersed in sterile water for 30 min before being subjected to a new identical PDI cycle. In this way, the antibacterial performance of the same films was systematically evaluated at first use, second use, and third use. Moreover, possible sublethal effects induced by the treatments were assessed by evaluating bacterial growth both onto solid and in liquid culture media.

(i) Growth onto solid medium: bacterial suspensions were serially diluted in MRD, and 100-μL aliquots from each dilution were spread plated onto PCA agar. The plates were incubated at 37 °C for 24 h. At the end of the incubation interval, for each treatment, one plate containing between 20 and 200 colonies was photographed inside an image acquisition chamber (Immagini & Computer, Bareggio, Milan) using a digital EOS 550D camera (Canon, Milan). The camera was positioned 50 cm above the plate, which was highlighted against a black background and illuminated with satin photographic reflectors (4100 W). The images were digitized using the EOS UTILITY software (Canon, version 3.3.0) and saved as JPEGs. Microscope-acquired images were analyzed using Image Pro Plus software (version 6.3, Media Cybernetics, Inc., Bethesda, MD, USA), which enabled the determination of the diameter of each object (single colony).

(ii) Growth in liquid medium: turbidimetric growth curves were obtained by inoculating 10 μL of bacterial suspensions into 190 μL of BHI supplemented with 5% NaCl (*w/v*), distributed in duplicate in a U-bottom 96-well microtiter plate (Corning Life Science, NY). Non-inoculated wells served as blanks. The plate was incubated at 37 °C for 24 h, and optical density at 630 nm (OD_{630}) was monitored every 30 min using a Sunrise microplate reader (Tecan, Milan, Italy). Data were modelled using the online tool DMfit (https://combasebrowser.errc.ars.usda.gov/DMFit.aspx), which provided estimates of lag time (λ, h), maximum specific growth rate (μ_{max}, OD/h), and final cell density (OD).

2.5. Determination of VP'S ability to generate reactive oxygen species

ROS generation was evaluated by probing representative species associated with both Type I and Type II photodynamic pathways.

2.5.1. Singlet oxygen generation

The potential generation of singlet oxygen by VP under visible light was evaluated using 9,10-anthracenedipropionic acid (ADPA) as a selective chemical probe [27]. An aqueous solution of ADPA (1.11×10^{-5} mol L^{-1}, 3.0 mL) was transferred into two quartz cuvettes suitable for UV–Vis spectrophotometry. Rectangular sections (10.0 × 25.0 mm) of VP, either pristine or reused (after two or three treatment cycles), were placed in one cuvette, whereas the second served as a control without material. Initial absorbance spectra were recorded at 377 nm (t_0), followed by exposure of both cuvettes to blue light from an LED source with maximum emission wavelength of 470 nm and an irradiance of 100 W m^{-2}. Samples were magnetically stirred during irradiation, and spectra were acquired at 10, 20, 30, 60, and 90 min. Oxidation of ADPA was expressed as $\ln(I_0/I)$ versus time, where I_0 and I denote the absorbance at 377 nm before and after irradiation, respectively. All experiments were performed in duplicate.

2.5.2. Hydroxyl and hydroperoxyl radicals generation

To investigate the production of hydroxyl and hydroperoxyl radicals, a method based on the oxidation of indigo carmine as a radical probe was employed [29]. A 3 mL aliquot of an aqueous solution of indigo-5,5′-disulfonic acid disodium salt (5 μM) was transferred into a quartz cuvette, and a rectangular section (10.0 × 25.0 mm) of VP, either pristine or reused after two or three treatment cycles, was immersed in the solution. The cuvette was exposed to blue LED light as previously described. At 10, 20, 30, 60, and 90 min, the film was removed, and the UV–Vis spectrum was recorded. The absorbance at 610 nm was used to monitor the dye decomposition. To evaluate the dye's photostability under the same irradiation conditions, control measurements were performed with the dye solution alone (without the film). All experiments were conducted at two pH values (6.0 and 5.0, adjusted using HCl, 0.1 M) and repeated in duplicate.

2.5.3. Hydrogen peroxide generation

The concentration of hydrogen peroxide (H_2O_2) was determined using a colorimetric assay based on titanium(IV) sulfate complexation, using a procedure already described [30].

The titanium reagent was prepared by dissolving TiO_2 (1 g) into concentrated H_2SO_4 (95%, 100 mL) under stirring at 155 °C for 24 h. The mixture was then filtered to remove undissolved TiO_2, yielding a clear Ti^{4+}-rich solution. Upon reaction with H_2O_2, this reagent forms a yellow peroxo-titanium complex, whose intensity correlates with peroxide concentration according to the following simplified reaction. A calibration curve was obtained using H_2O_2 solutions at concentrations of 10.9, 1.09, 0.109, and 0.0109 g L^{-1}. For each sample (5.0 mL), titanium reagent solution (1.0 mL) was added under stirring, and allowed to react for 5 min. The mixtures were transferred into quartz cuvettes, and the UV–Vis absorbance was recorded at 410 nm. To assess whether VP films generated H_2O_2 upon illumination, five separate vials were prepared, each containing two VP film strips (10.0 × 25.0 mm) immersed into 7 mL of Milli-Q water. Each vial was then irradiated with blue LED light for 10, 20, 30, 60, or 90 min. Immediately after the designated illumination time, 5.0 mL of the solution from each vial was withdrawn, mixed with titanium reagent (1.0 mL) under stirring, and allowed to react for 5 min. The H_2O_2 content was then determined by measuring the absorbance at 410 nm. All experiments were conducted in duplicate.

2.6 Specific surface area and porosity measurements

The specific surface area (SSA) of the samples was determined by nitrogen adsorption with a Micrometrics TriStar II Plus, outgassed at 150 °C. The SSA was determined by the Brunauer, Emmett and Teller method (BET), and pore area and volume distribution for pores between 8.5 and 1500.0 Å radius by the Barrett-Joyner-Halenda (BJH) method.

2.6. Scanning electron microscopy (SEM)

Morphological observations were performed on both microbial cells and VP films.

The morphological analysis of bacterial cells was performed using scanning field-emission scanning electron microscopy (FE-SEM, JEOL JSM7610F+, Tokyo, Japan). Samples were mounted on specimen holders with copper tape and coated with gold using a Sputter Coater 108 auto (Cressington Scientific Instruments Ltd., Watford, UK). Briefly, after the different treatments, 10 μL of each bacterial suspension was deposited onto a stainless-steel stub and processed for SEM observation. Cells were allowed to adhere, then fixed in 2.5% (*v*/v) glutaraldehyde for 1 h at room temperature. Samples were then rinsed three times with phosphate-buffered saline (PBS) and sequentially dehydrated through a graded ethanol series (50%, 70%, 90%, and 100%), with each step lasting 15 min. After dehydration, samples were sputter-coated with a thin layer of gold to enhance conductivity. SEM imaging was conducted using an acceleration voltage of 5 kV and a working distance of 12 mm. To avoid hydration artifacts, all samples were stored in a silica-containing desiccator and imaged immediately after removal. For each condition, images were acquired from at least three distinct regions to ensure representative morphological observations.

The morphological analysis of the VP films was performed using a EVO 40 system SEM (Carl Zeiss, Milan, Italy). These samples were sputter-coated with a thin layer of gold as well. Imaging was conducted using an acceleration voltage of 20 kV and an average working distance of 11 mm.

Observations on both microbial cells and on VP films were conducted using secondary electrons.

2.7. Statistical analysis

All experiments were performed in three independent biological replicates. For each biological replicate, two technical replicates were included, as specified in the corresponding assay. Statistical analysis was performed on the biological replicates, while technical replicates were used to increase measurement robustness within each experiment. Results are expressed as mean ± standard deviation (SD). One-way analysis of variance was carried out, and differences between the means were assessed using Tukey's HSD *post-hoc* test ($p < 0.05$) by using R v.4.3.3 for Windows (The R Foundation for Statistical Computing).

3. Results and discussion

3.1. Effect of VP films in the dark: Viability, colony morphology, and growth kinetics

To investigate whether VP films possess intrinsic antibacterial activity, *S. aureus* suspensions were incubated with VP for 90 min in the dark. Fig. 1 shows that bacterial viability remained close to the initial values throughout the incubation time. This was observed not only in the untreated control but also in the presence of VP films during their first, second, and third uses. In particular, no time-dependent reduction in CFU was detected, and no worsening of the antibacterial effect was associated with film reuse. The small variations observed among conditions fell within the experimental variability and were not statistically significant ($p > 0.05$). These results confirm that VP is non-bactericidal under the tested dark conditions. This result differs from data reported in the literature on vanillin-based polyimine materials, which show intrinsic antibacterial activity under dark conditions [22]. However, those systems are structurally different from VP and were tested under markedly different exposure conditions. In particular, in those studies bacterial cells were placed in direct contact with the polymer surface, whereas in the present work the interaction occurred in an aqueous suspension, where contact with the film was necessarily solution-mediated. These differences in both material design and cell-polymer exposure conditions may account for the observed differences in antibacterial behaviour.

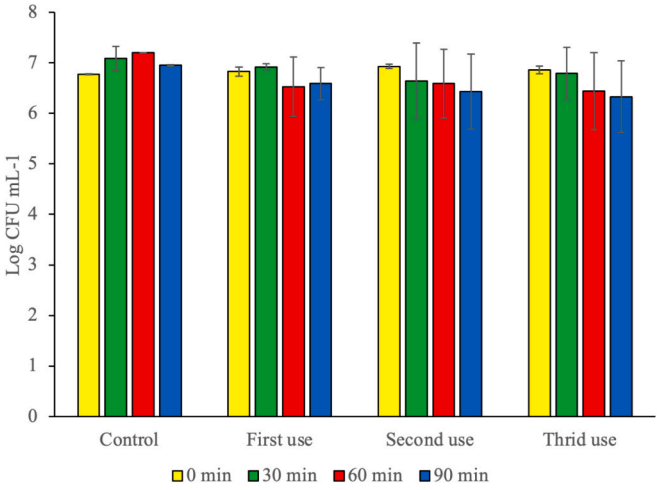

Fig. 1. *S. aureus* viability (Log CFU mL^{-1}) in the presence of VP films used one, two and three times in the dark condition. Data are shown as mean ± SD from three independent biological replicates; each biological replicate included two technical replicates. Control refers to a microbial suspension exposed under the same irradiated conditions.

However, the absence of lethality does not exclude the induction of sublethal stress. Visual inspection of agar plates revealed a marked alteration in colony morphology: colonies from dark controls displayed normal size, whereas those from VP-treated suspensions appeared noticeably smaller. Image-based analysis confirmed this scenario: control cultures produced colonies of typical diameter (1135.1 μm ± 55.6), while VP-treated cultures generated considerably smaller colonies (174.1 μm ± 18.3) (Fig. 2). Such a reduction is fully consistent with documented responses of sublethally injured bacteria, which exhibit delayed outgrowth and smaller colony size due to impaired metabolic activity [31,32].

To further characterize this physiological impairment, microbial suspensions exposed to VP in the dark were subjected to turbidimetric growth-curve analysis (Fig. 3).

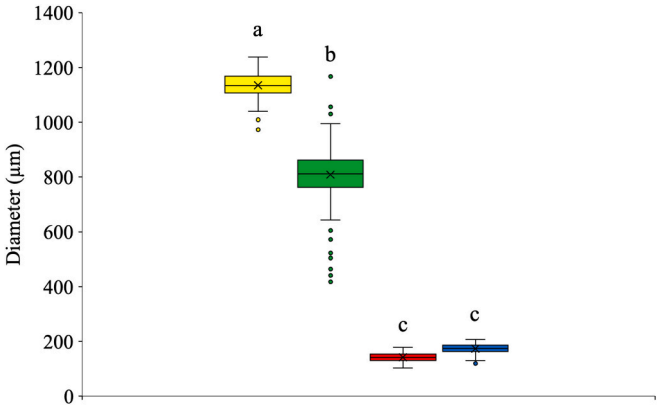

Fig. 2. *S. aureus* colony diameter; control in the dark (yellow), control irradiated (green), exposed to VP at its first use in the dark (red), and exposed to VP and irradiated (blue). Samples were irradiated by means of a blue LED lamp (λ_{max} = 470 nm, fluence rate 100 W m^{-2}). Data are shown as mean from three independent biological replicates; each biological replicate included two technical replicates. Different letters indicate statistically different means ($p < 0.05$). (For interpretation of the references to colour in this figure legend, the reader is referred to the web version of this article.)

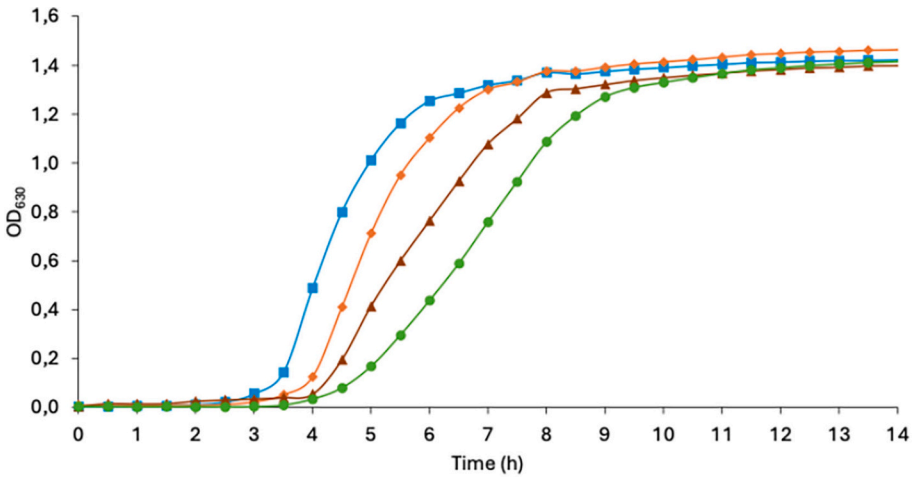

Fig. 3. Turbidimetric growth curves of *S. aureus*; control in the dark (blue), control irradiated (orange), exposed to VP at its first use in the dark (red), exposed to VP and irradiated (green). Samples were irradiated by means of a blue LED lamp (λ_{max} = 470 nm, fluence rate 100 W m^{-2}). Data are shown as mean from three independent biological replicates; each biological replicate included two technical replicates. (For interpretation of the references to colour in this figure legend, the reader is referred to the web version of this article.)

Table 1
Growth parameters (lag phase (λ, h); maximum growth rate (μ_{max}, OD/h); and final cell density (OD) of *S. aureus* in the presence of VP and absence (control) in the light condition (90 min, 100 W/m^2, λ = 470 nm) and in the dark; within the same sample, different letters indicate statistically different means ($p < 0.05$).

	λ (h)	μ_{max} (OD/h)	Final cell density OD
Control-dark	$3.14^{d} \pm 0.08$	$0.53^{a} \pm 0.05$	$1.49^{a} \pm 0.04$
Control-light	$3.66^{c} \pm 0.12$	$0.48^{a} \pm 0.06$	$1.52^{a} \pm 0.03$
VP-dark	$3.98^{b} \pm 0.06$	$0.36^{b} \pm 0.01$	$1.47^{a} \pm 0.01$
VP-light	$4.48^{a} \pm 0.63$	$0.35^{b} \pm 0.02$	$1.49^{a} \pm 0.01$

Growth-curve modelling (Table 1) revealed a significantly prolonged lag phase (λ = 3.98 h vs. 3.14 h in controls) and a reduced maximum specific growth rate (μ_{max} = 0.36 vs. 0.53 OD/h).

These alterations indicate that contact with VP slows down the transition to active growth and reduces replication efficiency. Notably enough, the amplitude of the stationary phase remained unchanged, suggesting that cells eventually recovered when transferred to a nutrient-rich medium. Overall, VP induces sublethal stress sufficient to impair early physiological processes, while remaining non-bactericidal in the dark. The observations from this study are consistent with previous reports showing that contact-mediated toxicity of polyimines can impair bacterial cells by damaging their membranes, even in the absence of immediate bactericidal effects [21,22]. Since membrane integrity is crucial for microbial viability, sublethal injury at this level may still be repairable, but only at the expense of additional time and metabolic effort. As a result, exposed cells may retain the ability to recover in nutrient-rich conditions while displaying delayed entry into exponential growth, as reflected by the prolonged lag phase observed in the present study.

3.2. *Effect of blue light and VP + blue light: Viability, colony morphology, and growth kinetics*

The potential of VP-induced sublethal stress to sensitize *S. aureus* to blue-light-mediated oxidative mechanisms was subsequently assessed. Blue light in the 405–450 nm region is known to efficiently inactivate bacteria due to strong porphyrin absorption [7], whereas at longer wavelengths, such as 460–470 nm, antimicrobial efficacy sharply declines and fluences above 100 J cm^{-2} are typically required [12,14]. We deliberately used subthreshold irradiation (470 nm; 18, 36, and 54 J cm^{-2}) to test whether a VP-associated enhancement could be detected under conditions in which light alone was expected to remain weakly effective. This choice should be regarded as a mechanistic probing strategy rather than as an attempt to optimize bactericidal performance. In this sense, 470 nm irradiation at moderate fluences was not selected as an optimized application condition, but as a mild irradiation regime in which any VP-mediated enhancement could be more clearly resolved. Such an approach may also be of interest for the future treatment of light-sensitive matrices, where preserving product quality may be as important as antimicrobial efficacy.

Control experiments confirmed that 470 nm irradiation alone did not significantly affect viability ($p > 0.05$; Fig. 4) with viable counts remaining close to the initial value throughout the treatment. Nonetheless, colonies from light-only treatments were significantly smaller than those from dark controls ($p < 0.05$), indicating that irradiation alone caused mild sublethal stress (Fig. 2). Colony size heterogeneity increased markedly under light exposure, likely reflecting physiological

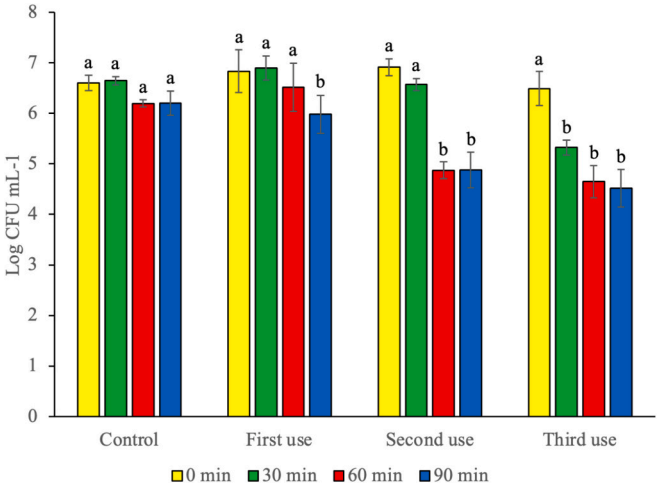

Fig. 4. *S. aureus* viability (Log CFU mL^{-1}) in the presence of VP films used one, two, and three times (blue LED light, fluence rate of 100 W m^{-2}). Control refers to a microbial suspension exposed under the same irradiated conditions. Data are shown as mean ± SD from three independent biological replicates; each biological replicate included two technical replicates. Within the same sample, different letters indicate statistically different means ($p < 0.05$). (For interpretation of the references to colour in this figure legend, the reader is referred to the web version of this article.)

difference in endogenous chromophore content: actively growing cells, richer in porphyrins and flavins, generate more ROS under irradiation and thus are more sensitive, whereas stationary-phase cells exhibit lower susceptibility [11,33].

The combination of VP and blue light produced markedly different outcomes. Colonies arising from VP + light suspensions were significantly smaller than those from light-alone conditions and comparable in size to those formed after VP exposure in the dark, indicating that VP remains the primary inducer of morphological stress. Nevertheless, despite similar colony morphology, the viability outcomes diverged sharply: VP in combination with light produced a measurable bactericidal effect, with the magnitude of killing increasing with film reuse (Fig. 4). More specifically, after the first use of VP, viability remained comparable to that of the irradiated control up to 60 min, whereas a significant reduction was observed only after 90 min, indicating a limited antibacterial effect under these conditions. By contrast, second-use VP films produced a marked decrease in viability already after 60 min (36 J cm^{-2}), which was maintained at 90 min and corresponded to an approximately 2-log reduction relative to the initial count. Third-use VP films showed the strongest and fastest effect, with a significant decline already after 30 min (18 J cm^{-2}), followed by a further decrease at 60 and 90 min, ultimately approaching a 2-log reduction. Overall, these data indicate that repeated reuse progressively enhances the antibacterial response associated with VP under blue-light irradiation, reducing both the exposure time and the fluence required to obtain a measurable effect.

Growth-curve analysis further substantiated this observation. As shown in Fig. 3 and Table 1, both light exposure and VP contact independently extended the lag phase, but the combined VP + light condition produced the most pronounced effect. Specifically, lag time increased by 22% relative to the light control and 12% relative to VP-dark, indicating cumulative interference with cellular repair and adaptation. When considered together, the viability data, colony-size analysis, and growth-curve modelling are consistent with a division of roles within the inactivation mechanism:

(i) the polyimine matrix induces membrane-associated sublethal stress, and.

(ii) blue light triggers porphyrin-mediated oxidative damage, thereby contributing to cell killing [7].

Although the latter effect was not demonstrated in this study, it remains mechanistically plausible based on the widely accepted antimicrobial mechanism of blue light [7]. The reduction in colony size would therefore be attributable mainly to VP-induced stress, whereas the bactericidal outcome would arise from the additional oxidative challenge imposed by irradiation.

3.3. Structural drivers and mechanistic basis of VP-enhanced blue-light antibacterial activity

Before examining structural changes in VP films, it was necessary to clarify whether the observed light-dependent antibacterial effect could arise from a conventional photodynamic mechanism. Based on our previous experience with photodynamic inactivation [16,17,26,27], we initially considered the possibility that minor photoactive species might form during thermal processing of the polymer. However, neither polyimines nor vanillin-derived structures are known to possess intrinsic photoreactivity. Standard assays for singlet oxygen, radical species, and hydrogen peroxide failed to detect measurable ROS generation by VP under the tested conditions (Fig. S3). These results indicate that VP does not behave as a conventional photosensitizer. However, the formation of short-lived, surface-confined, or impurity-derived reactive species below the detection limit of the applied assays cannot be completely excluded. Given their very short lifetime and limited diffusion range, such species are unlikely to account for the observed multi-log reduction in bacterial viability in the absence of sustained generation or direct cell-surface interactions. In particular, the Ti(IV)-based assay used for H_2O_2 determination was calibrated down to ca. 11 mg/L; trace peroxide formation below this range may therefore remain undetected. Even so, such trace levels would be unlikely to account for the observed multi-log reduction in bacterial viability, since this concentration range is well below H_2O_2 levels typically associated with substantial killing of *S. aureus* in vitro [34]. Importantly, the absence of detectable ROS production by VP indicates that the polymer itself does not behave as a conventional photosensitizer under the tested conditions. At the same time, the antibacterial effect observed under VP + light treatment suggests that light-dependent bacterial inactivation can still occur in the presence of the material. Because blue light is known to act through excitation of endogenous bacterial chromophores, especially porphyrins, and because *S. aureus* contains such intracellular porphyrins [35], the most plausible interpretation is that VP increases bacterial susceptibility to endogenous photo-oxidative damage triggered by 470 nm irradiation. This mechanism should, however, be regarded as a data-supported working hypothesis rather than a direct mechanistic demonstration. In addition, a previously reported leachate-control experiment performed on this material argues against the contribution of diffusible species released during irradiation [24]. In that test, films were irradiated in PBS, then removed, and the recovered solution showed no detectable antimicrobial activity against *S. aureus under irradiation*, supporting the view that direct contact with the polymer is required for the observed light-enhanced effect.

Having excluded a photodynamic contribution from the polymer itself, we next investigated whether mechanical and structural changes arising during film reuse could explain the progressive amplification of the inactivation effect. SEM observations (Fig. S4) suggested that repeated handling and irradiation cycles induce microcracks in VP films, potentially increasing accessible surface area and enhancing polymer-bacteria interactions. To verify this hypothesis, pristine and reused films were characterized using nitrogen adsorption–desorption techniques.

By IUPAC definitions, microporosity is pores <2 nm diameter, mesoporosity is between 2 and 50 nm diameter and macroporosity is >50 nm diameter [36]. BET measurements revealed that the specific surface area nearly doubled upon reuse, increasing from 12.94 $m^2\ g^{-1}$ for pristine films to 21.82 $m^2\ g^{-1}$ for reused samples, a 70% increase in SSA (Fig. 5a-b). More detailed BJH analyses, focusing on mesopores and small macropores in the 1.2–120 nm radius range, confirmed this trend: the surface area attributable to these pores increased by 75% after reuse. The average pore radius remained unchanged at ca. 3 nm (ca. 6 nm diameter), however, with 80% of the mesopores being under 8.8 nm in diameter by area in both cases, indicating that reuse does not alter the pore size distribution but rather the overall accessible surface area, due to the microcracking/fracturing.

The BJH pore volume data similarly showed an increase upon reuse: from 0.10 $cm^3\ g^{-1}$ (pristine) to 0.18 $cm^3\ g^{-1}$ (reused), an 80% increase in pore volume (Fig. 5c-d). Larger pores contribute much more to the volume than smaller ones, as a doubling of radius leads to a volume eight times greater for a spherical pore, for instance. However, as shown in Fig. 5c-d there was no significant difference in the pore radius distribution by volume before and after use. Given that BJH analysis selectively evaluates mesopores and excludes micropores (<2 nm), which were not reliably detected by BET analysis, these data likely provide a more accurate representation of the mesoporous contribution to antibacterial performance. Both in the pristine sample and after reuse, 80% of the mesopore volume was from pores <18 nm in diameter, again showing no significant change in the pore-size distribution, only an increase in the number of available pores by 80%.

Collectively, these findings indicate that reuse increases VP's accessible surface area without significantly altering the pore-size distribution. This apparent decoupling between surface area and pore-size distribution can be rationalised by considering the microstructural changes induced during film reuse (Fig. S4). Mechanical handling and repeated cycles likely generate new microfractures, exposing previously inaccessible internal

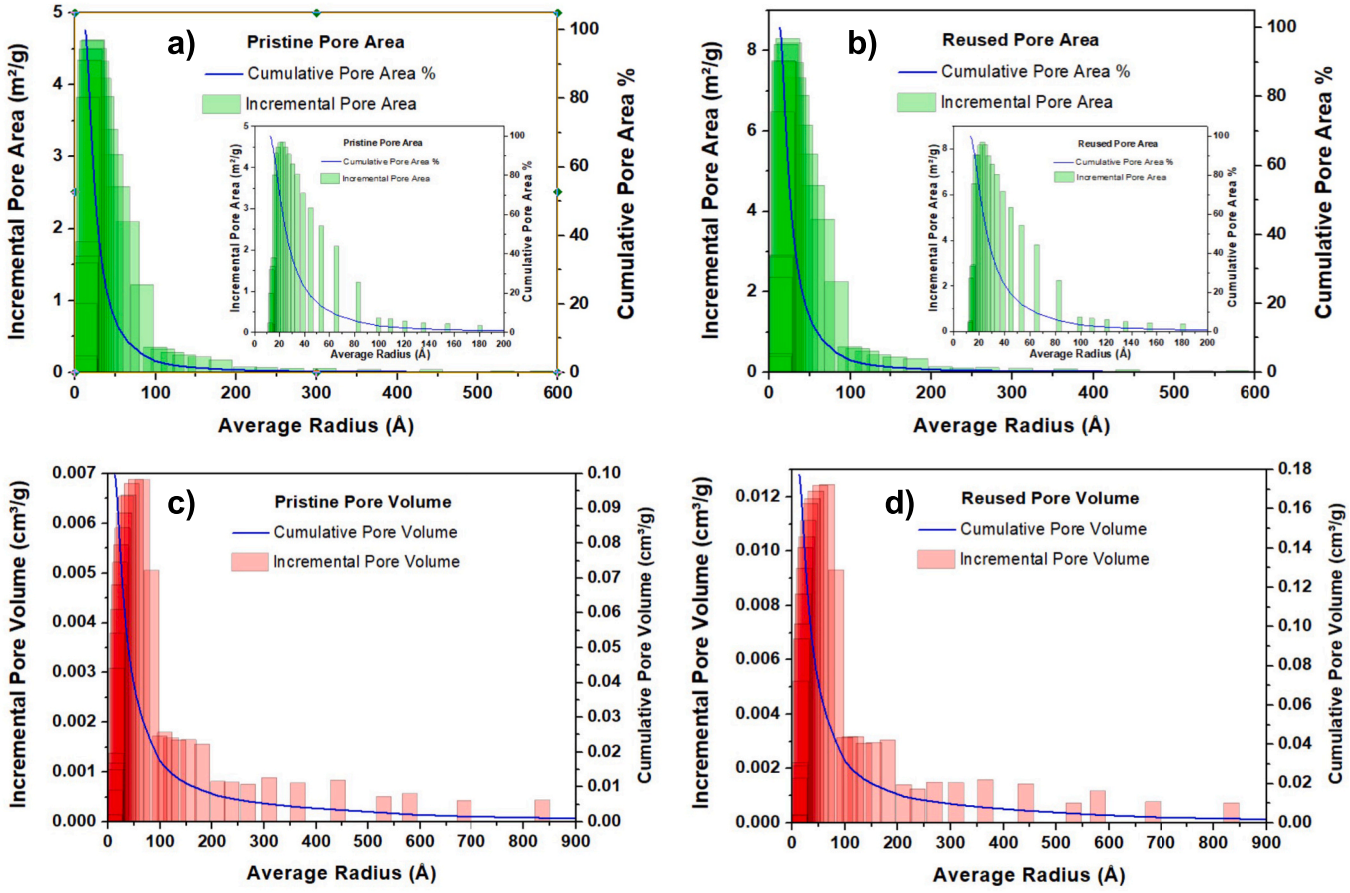

Fig. 5. BJH pore size distributions by pore area (a, b) and pore volume (c, d) for pristine (a, b) and reused at third use (b, d) samples. The insets in a) and b) show the pore area size distribution between 0 and 200 Å radius (0–40 nm diameter).

surfaces and thereby increasing the total accessible surface area without substantially modifying the intrinsic dimensions of the pre-existing mesopores. This structural evolution may increase the extent of the contact interface between bacterial cells and the polyimine matrix. At the same time, a rougher and more fractured surface may also favour greater cell retention or adhesion during treatment. In this sense, the reuse-dependent enhancement in antibacterial activity can be interpreted more cautiously as consistent with an increased contact-mediated contribution to the observed additive effect under irradiation, rather than as evidence of a uniquely defined mechanism.

Following the structural analysis, SEM imaging provided qualitative support for the proposed mechanism. Cells maintained in the dark without VP exhibited smooth and intact morphology (Fig. 6A), in agreement with previous observations [37,38]. Cells exposed to light alone (Fig. 6B) showed occasional morphological alterations, whereas cells exposed to VP in the dark (Fig. 6C) appeared overall similar to the dark control, without clear evidence of extensive membrane damage. By contrast, the combined VP + light condition (Fig. 6D) showed the most evident structural alterations, including cell deformation and lysis, consistent with greater cell damage under the combined treatment. Unlike classical cationic polymers, whose antimicrobial activity stems from electrostatic disruption, VP is expected to remain largely uncharged at physiological pH, given the reported pKa values of imines [39]. Therefore, its interaction with bacterial membranes likely proceeds through hydrogen bonding and hydrophobic interactions, leading to subtle but physiologically meaningful membrane stress. This stress primes bacteria by weakening their repair and growth capacities, thereby enhancing their vulnerability to ROS generated intracellularly via porphyrin photoactivation.

Overall, the collective evidence supports a working model in which VP does not act as a photoactive antibacterial material, but rather as a mechanical and physiological sensitizer that amplifies the bactericidal action of blue light. In this model, contact-induced sublethal stress and endogenous porphyrin photoactivation converge to promote microbial inactivation at irradiation doses that would otherwise be only weakly effective. However, the present study does not establish a formal structure-activity relationship, and further comparative studies on structurally related polyimines will be necessary to identify the specific chemical determinants of this effect.

4. Conclusions

Rather than introducing a new polymer chemistry, the present study demonstrates a new functional role for the previously reported vanillin-derived polyimine VP. Specifically, polymer-cell interactions can significantly influence antibacterial outcomes under visible light even when the polymer itself lacks intrinsic photoactivity. In the specific case of VP, contact with the polymer matrix induces a reproducible sublethal stress that alters bacterial response to subsequent oxidative challenges. The present data do not support a direct ROS-generating role of the polymer under the tested conditions, although minor contributions from undetected reactive species cannot be fully excluded. The progressive enhancement of antibacterial efficacy observed upon material reuse further indicates that structural evolution of dynamic polymer networks during operation can contribute to functional performance. The increase in accessible surface area without detectable changes in pore-size distribution suggests that microstructural rearrangements, rather than chemical modification,

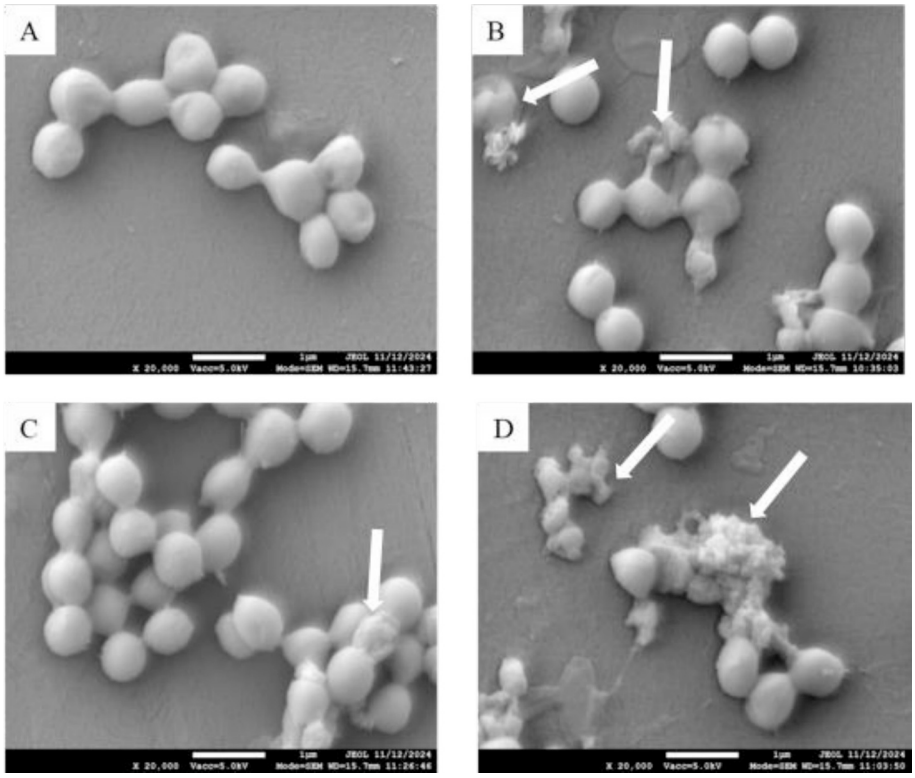

Fig. 6. *S. aureus* cell SEM micrographs (20,000× magnification) obtained using the VP film at its **first use**: dark control (A); light control (B): dark VP-exposed (C): light VP-exposed (D). For SEM observation, treated cells were deposited onto a stainless-steel stub. White arrows indicate cell deformation and lysis.

govern the strengthening of polymer-microbe interactions. From a polymer science perspective, these findings support the idea that dynamic covalent materials can be engineered not only for recyclability or self-healing, but also to modulate interfacial biological responses. While demonstrated here using *Staphylococcus aureus* as a model system, this approach provides a framework for the rational design of reusable polymeric materials that enhance light-mediated antibacterial processes under mild irradiation conditions. A further strength of the study lies in the combined use of complementary biological, morphological, and structural analyses, which together support a coherent interpretation of the observed material-assisted antibacterial response. These findings define a proof-of-concept framework in which a neutral polyimine can enhance antibacterial response to blue light through a contact-mediated sensitizing effect. Within this framework, the proposed mechanism is best regarded as a data-supported working model that identifies plausible structure–function relationships and provides a basis for further mechanistic refinement. Under the selected irradiation conditions, the absolute reduction in bacterial viability remains modest. However, this limitation should be viewed in light of the purpose of the study, which was not to optimize bactericidal performance but to determine whether VP could modulate bacterial response to blue light. The advance of the study is therefore conceptual and functional rather than performance-based: it identifies a previously unreported contact-dependent sensitizing role of a neutral, non-photoactive polyimine under blue-light exposure. Future studies on systematically modified polyimine analogues may help clarify which structural features govern the priming-plus-light behaviour. The broader activity spectrum of VP also remains an important area for further investigation, particularly with respect to other bacterial species, resistant strains, and fungi. From an application perspective, these findings may be relevant to scenarios in which bacterial-load reduction is sought as a complementary control measure rather than absolute sterility, such as food-processing or environmental settings, or the periodic treatment of material and container surfaces under blue light in combination with conventional cleaning procedures.

CRediT authorship contribution statement

Marilena Marino: Validation, Supervision, Resources, Methodology, Data curation, Conceptualization, Writing – review & editing, Writing – original draft. **Elisabetta Gover:** Methodology, Investigation, Formal analysis, Writing – review & editing, Writing – original draft. **Asja Brovedani:** Investigation, Formal analysis, Data curation, Writing – review & editing, Writing – original draft. **Robert C. Pullar:** Validation, Supervision, Methodology, Investigation, Formal analysis, Data curation, Conceptualization, Writing – review & editing, Writing – original draft. **Daniele Goi:** Supervision, Funding acquisition, Data curation, Writing – review & editing. **Francesco Andreatta:** Investigation, Data curation, Writing – review & editing. **Alfredo Rondinella:** Investigation, Formal analysis, Data curation, Conceptualization, Writing – review & editing, Writing – original draft. **Paolo Strazzolini:** Methodology, Data curation, Conceptualization, Writing – review & editing, Writing – original draft. **Clara Comuzzi:** Visualization, Validation, Supervision, Methodology, Data curation, Conceptualization, Writing – review & editing, Writing – original draft.

Declaration of generative AI and AI-assisted technologies in the writing process

During the preparation of this work the authors used Grammarly in order to improve the language and the readability of the manuscript. After using this tool, the authors reviewed and edited the content as needed and took full responsibility for the content of the publication.

Declaration of competing interest

The authors declare no conflict of interest.

Acknowledgments

The Authors thank Dr. Paolo Martinuzzi for contributing to NMR measurements and Dr. Pierluigi Polese for precious technical assistance.

Appendix A. Supplementary data

Supplementary data to this article can be found online at https://doi.org/10.1016/j.jphotobiol.2026.113494.

Data availability

Data will be made available on request.

References

[1] C. Muoghalu, H.C. Kaboggoza, S. Semiyaga, S. Lebu, C. Liu, C. Niwagaba, F. Nansubuga, M. Manga, Antibiotic resistant bacteria (ARB) and genes (ARGs) in urban wastewater treatment plants: influencing factors, mechanisms, and removal efficiency, Environ. Pollut. 383 (2025), https://doi.org/10.1016/j.envpol.2025.126851.

[2] A.K. Pandey, Sustainable water management through integrated technologies and circular resource recovery, Environ. Sci. (Camb.) 11 (2025) 1822–1846, https://doi.org/10.1039/d5ew00103j.

[3] N. Dhanda, S. Kumar, Water disinfection and disinfection by products, Environ. Monit. Assess. 197 (2025), https://doi.org/10.1007/s10661-025-13915-9.

[4] S.L. Miller, J. Linnes, J. Luongo, Ultraviolet germicidal irradiation: future directions for air disinfection and building applications, Photochem. Photobiol. (2013) 777–781, https://doi.org/10.1111/php.12080.

[5] L.M. Vasilyak, Ultrasound application in systems for the disinfection of water, Surf. Eng. Appl. Electrochem. 46 (2010) 489–493, https://doi.org/10.3103/S1068375510050133.

[6] A. Parkinson, M.J. Barry, F.A. Roddick, M.D. Hobday, Preliminary toxicity assessment of water after treatment with UV-irradiation and UVC/H 2 O 2, Water Res. 35 (2001) 3656–3664.

[7] A. Lena, M. Marino, M. Manzano, C. Comuzzi, M. Maifreni, An overview of the application of blue light-emitting diodes as a non-thermic green Technology for Microbial Inactivation in the food sector, Food Eng. Rev. 16 (2024) 59–84, https://doi.org/10.1007/s12393-023-09355-1.

[8] V. Lucarelli, D. Amodeo, I. de Palma, N. Nante, G. Cevenini, G. Messina, The potential role of violet-blue light to preventing hospital acquired infections: a systematic review, Front. Public Health 12 (2024), https://doi.org/10.3389/fpubh.2024.1474295.

[9] J. Wu, Z. Chu, Z. Ruan, X. Wang, T. Dai, X. Hu, Changes of intracellular porphyrin, reactive oxygen species, and fatty acids profiles during inactivation of methicillin-resistant Staphylococcus aureus by antimicrobial blue light, Front. Physiol. 9 (2018), https://doi.org/10.3389/fphys.2018.01658.

[10] J.E. Hyun, S.K. Moon, S.Y. Lee, Antibacterial activity and mechanism of 460–470 nm light-emitting diodes against pathogenic bacteria and spoilage bacteria at different temperatures, Food Control 123 (2021), https://doi.org/10.1016/j.foodcont.2020.107721.

[11] C. dos Anjos, L.G. Leanse, M.S. Ribeiro, F.P. Sellera, M. Dropa, V.E. Arana-Chavez, N. Lincopan, M.S. Baptista, F.C. Pogliani, T. Dai, C.P. Sabino, New insights into the bacterial targets of antimicrobial blue light, Microbiol. Spectrum 11 (2023), https://doi.org/10.1128/spectrum.02833-22.

[12] R.M. Tomb, T.A. White, J.E. Coia, J.G. Anderson, S.J. MacGregor, M. Maclean, Review of the comparative susceptibility of microbial species to photoinactivation using 380–480 nm violet-blue light, Photochem. Photobiol. 94 (2018) 445–458, https://doi.org/10.1111/php.12883.

[13] J. Schmid, K. Hoenes, P. Vatter, M. Hessling, Antimicrobial effect of visible light—photoinactivation of legionella rubrilucens by irradiation at 450, 470, and 620 nm, Antibiotics 8 (2019), https://doi.org/10.3390/antibiotics8040187.

[14] A. Lena, C. Comuzzi, M. Manzano, M. Maifreni, Effect of blue light at different wavelengths on the inactivation of foodborne bacteria: evaluation of microbial susceptibility, Food Microbiol. 137 (2026), https://doi.org/10.1016/j.fm.2026.105052.

[15] R. Allen, Y. Somorin, M. Slemon, E. Zekaite, C. Haugh, C. Hobbs, M.S. Zeden, J. P. O'Gara, C. O'Byrne, A low acriflavine dose strongly potentiates the antimicrobial effect of blue light on Staphylococcus aureus, J. Photochem. Photobiol., A 28 (2025), https://doi.org/10.1016/j.jpap.2025.100264.

[16] M. Thandu, G. Rossi, D. Goi, P. Guerriero, D. Poletti, P. Strazzolini, C. Comuzzi, Synthesis, characterization, and photodynamic activity of new antimicrobial PVC based composite materials, Eur. Polym. J. 160 (2021), https://doi.org/10.1016/j.eurpolymj.2021.110805.

[17] C. Comuzzi, M. Marino, D. Poletti, M. Boaro, P. Strazzolini, New antimicrobial PVC composites. Porphyrins self-aggregation in tuning surface morphologies and photodynamic inactivation towards sustainable water disinfection, J. Photochem. Photobiol. A Chem. 430 (2022) 1–11, https://doi.org/10.1016/j.jphotochem.2022.113967.

[18] M. López, N.S. Gsponer, D.A. Heredia, E.N. Durantini, Chlorin-based photodynamic antimicrobial glass surfaces for the eradication of Staphylococcus aureus, Surf. Interfaces 66 (2025), https://doi.org/10.1016/j.surfin.2025.106575.

[19] F.E. Akram, T. El-Tayeb, K. Abou-Aisha, M. El-Azizi, A combination of silver nanoparticles and visible blue light enhances the antibacterial efficacy of ineffective antibiotics against methicillin-resistant Staphylococcus aureus (MRSA), Ann. Clin. Microbiol. Antimicrob. 15 (2016), https://doi.org/10.1186/s12941-016-0164-y.

[20] J. Xu, Y. Li, X. Zhou, Y. Li, Z. Da Gao, Y.Y. Song, P. Schmuki, Graphitic C3N4-sensitized TiO2 nanotube layers: a visible-light activated efficient metal-free antimicrobial platform, Chem. Eur. J. 22 (2016) 3947–3951, https://doi.org/10.1002/chem.201505173.

[21] P. Li, J. Zhang, J. Ma, C.A. Xu, X. Liang, T. Yuan, Y. Hu, Z. Yang, Fully bio-based thermosetting polyimine vitrimers with excellent adhesion, rapid self-healing, multi-recyclability and antibacterial ability, Ind. Crop. Prod. 204 (2023), https://doi.org/10.1016/j.indcrop.2023.117288.

[22] Y. Yang, Z. Xia, L. Huang, R. Wu, Z. Niu, W. Fan, Q. Dai, J. He, C. Bai, Renewable vanillin-based thermoplastic polybutadiene rubber: high strength, recyclability, self-welding, shape memory, and antibacterial properties, ACS Appl. Mater. Interfaces 14 (2022) 47025–47035, https://doi.org/10.1021/acsami.2c13339.

[23] K. McKenzie, M. Maclean, I.V. Timoshkin, S.J. MacGregor, J.G. Anderson, Enhanced inactivation of Escherichia coli and listeria monocytogenes by exposure to 405nm light under sub-lethal temperature, salt and acid stress conditions, Int. J. Food Microbiol. 170 (2014) 91–98, https://doi.org/10.1016/j.ijfoodmicro.2013.10.016.

[24] E. Gover, A. Rondinella, M. Marino, A. Brovedani, A. Tavani, M. Lopriore, M. Alongi, L. Manzocco, L. Fedrizzi, D. Goi, P. Strazzolini, C. Comuzzi, Vanillin-based photoactive materials: a sustainable approach to antimicrobial solutions, J. Photochem. Photobiol. A Chem. 468 (2025), https://doi.org/10.1016/j.jphotochem.2025.116501.

[25] G. Bisson, C. Comuzzi, E. Giordani, D. Poletti, M. Boaro, M. Marino, An exopolysaccharide from Leuconostoc mesenteroides showing interesting bioactivities versus foodborne microbial targets, Carbohydr. Polym. 301 (2023) 1–10, https://doi.org/10.1016/j.carbpol.2022.120363.

[26] M.M. Thandu, S. Cavalli, G. Rossi, C.B. Rizzardini, D. Goi, C. Comuzzi, Biological evaluation of a porphyrin-SPION nanoconjugate as an antimicrobial magnetic photosensitizer, J. Porphyrins Phthalocyanines 21 (2017) 581–588, https://doi.org/10.1142/S1088424617500560.

[27] C. Comuzzi, A. Fiorot, A. Baggio, M. Maifreni, P. Strazzolini, M. Marino, S. Susmel, Imprinting pentaphyrin on conductive electropolymerized dipyrromethane films: a new strategy towards the synthesis of photokilling materials, Chempluschem 85 (2020) 776–782, https://doi.org/10.1002/cplu.202000137.

[28] B. Herigstad, M. Hamilton, J. Heersink, How to optimize the drop plate method for enumerating bacteria, J. Microbiol. Methods 44 (2001) 121–129. www.elsevier.comrlocaterjmicmeth.

[29] H. Liao, D. Stenman, M. Jonsson, Study of indigo carmine as radical probe in photocatalysis, J. Photochem. Photobiol. A Chem. 202 (2009) 86–91, https://doi.org/10.1016/j.jphotochem.2008.11.008.

[30] S. Wang, Z. Xie, D. Zhu, S. Fu, Y. Wu, H. Yu, C. Lu, P. Zhou, M. Bonn, H.I. Wang, Q. Liao, H. Xu, X. Chen, C. Gu, Efficient photocatalytic production of hydrogen peroxide using dispersible and photoactive porous polymers, Nat. Commun. 14 (2023), https://doi.org/10.1038/s41467-023-42720-6.

[31] G.A. Dykes, Image analysis of colony size for investigating sublethal injury in listeria monocytogenes, J. Rapid Methods Autom. Microbiol. 7 (1999) 223–231, https://doi.org/10.1111/j.1745-4581.1999.tb00395.x.

[32] L. Shao, Y. Sun, B. Zou, Y. Zhao, X. Li, R. Dai, Sublethally injured microorganisms in food processing and preservation: quantification, formation, detection, resuscitation and adaption, Food Res. Int. 165 (2023), https://doi.org/10.1016/j.foodres.2023.112536.

[33] Y. Wang, X. Li, H. Chen, X. Yang, L. Guo, R. Ju, T. Dai, G. Li, Antimicrobial blue light inactivation of Pseudomonas aeruginosa: Unraveling the multifaceted impact of wavelength, growth stage, and medium composition, J. Photochem. Photobiol. B 259 (2024), https://doi.org/10.1016/j.jphotobiol.2024.113023.

[34] C.B. Wilson, W.M. Weaver, Comparative Susceptibility of Group B Streptococci and *Staphylococcus aureus* to Killing by Oxygen Metabolites. https://www.jstor.org/stable/30104683?seq=1&cid=pdf, 1985.

[35] R. Yang, Y. Xu, J. Xu, Y. Li, X. Wan, R. Kong, C. Ding, H. Tao, H.L. Wang, The transcriptional changes of LrgA discriminates the responsiveness of Staphylococcus aureus towards blue light from that of photodynamic inactivation, J. Photochem. Photobiol. B 258 (2024), https://doi.org/10.1016/j.jphotobiol.2024.112967.

[36] M. Thommes, K. Kaneko, A.V. Neimark, J.P. Olivier, F. Rodriguez-Reinoso, J. Rouquerol, K.S.W. Sing, Physisorption of gases, with special reference to the evaluation of surface area and pore size distribution (IUPAC technical report), Pure Appl. Chem. 87 (2015) 1051–1069, https://doi.org/10.1515/pac-2014-1117.

[37] S. Shen, T. Zhang, Y. Yuan, S. Lin, J. Xu, H. Ye, Effects of cinnamaldehyde on Escherichia coli and Staphylococcus aureus membrane, Food Control 47 (2015) 196–202, https://doi.org/10.1016/j.foodcont.2014.07.003.

[38] I. de P. Ribeiro, J.G. Pinto, B.M.N. Souza, A.G. Miñán, J. Ferreira-Strixino, Antimicrobial photodynamic therapy with curcumin on methicillin-resistant Staphylococcus aureus biofilm, Photodiagn. Photodyn. Ther. 37 (2022), https://doi.org/10.1016/j.pdpdt.2022.102729.

[39] S. Zhang, J. Hu, W. Shang, J. Guo, X. Cheng, S. Song, T. Liu, W. Liu, Y. Shi, Light-driven H2O2 production over redox-active imine-linked covalent organic frameworks, Adv. Powder Mater. 3 (2024), https://doi.org/10.1016/j.apmate.2024.100179.